




Article

Diarylphosphate as a New Route for Design of Highly Luminescent Ln Complexes

Alexey E. Kalugin ^{1,2}, Mikhail E. Minyaev ^{1,3}, Lada N. Puntus ^{1,4}, Ilya V. Taydakov ⁵, Evgenia A. Varaksina ^{1,5}, Konstantin A. Lyssenko ⁶, Ilya E. Nifant'ev ^{1,6} and Dmitrii M. Roitershtein ^{1,3,7,*}

¹ A.V. Topchiev Institute of Petrochemical Synthesis RAS, 119991 Moscow, Russia; alex.kalug@gmail.com (A.E.K.); mminyaev@mail.ru (M.E.M.); ladapuntus@gmail.com (L.N.P.); janiy92@yandex.ru (E.A.V.); inif@org.chem.msu.ru (I.E.N.)

² Moscow Institute of Physics and Technology (MIPT), 141701 Dolgoprudnyi, Moscow Region, Russia

³ N.D. Zelinsky Institute of Organic Chemistry, RAS, 119991 Moscow, Russia

⁴ V.A. Kotel'nikov Institute of Radioengineering and Electronics, RAS, 141190 Fryazino, Moscow Region, Russia

⁵ P.N. Lebedev Physical Institute, RAS, 119991 Moscow, Russia; taidakov@gmail.com

⁶ Chemistry Department, M.V. Lomonosov Moscow State University, 119991 Moscow, Russia; kostya@xray.ineos.ac.ru

⁷ National Research University Higher School of Economics, 101000 Moscow, Russia

* Correspondence: roiter@yandex.ru; Tel.: +7-916-373-3507

Received: 5 July 2020; Accepted: 25 August 2020; Published: 28 August 2020



Abstract: Organophosphate-chloride complexes $[(2,6\text{-}i\text{Pr}_2\text{C}_6\text{H}_3\text{-O})_2\text{POO}]_2\text{LnCl}(\text{CH}_3\text{OH})_4 \cdot 2\text{CH}_3\text{OH}$, Ln = Nd (1), Eu (2), Gd (3), and Tb (4) have been obtained and structurally characterized. Their reaction with 2,2':6',2''-terpyridine leads to the formation of 1:1 adducts $[(2,6\text{-}i\text{Pr}_2\text{C}_6\text{H}_3\text{-O})_2\text{POO}]_2\text{LnCl}(\text{terpy})(\text{H}_2\text{O})_2(\text{CH}_3\text{OH})$, Ln = Eu (5), Gd (6), Tb (7) with exception of Nd, where tris-diisopropylphenylphosphate complex $[(2,6\text{-}i\text{Pr}_2\text{C}_6\text{H}_3\text{-O})_2\text{POO}]_3\text{Nd}(\text{terpy})(\text{H}_2\text{O})(\text{CH}_3\text{OH})$ (8) was obtained due to the ligand metathesis. A bright luminescence observed for the Eu and Tb organophosphate complexes is the first example of an application of organophosphate ligands for 4f-ions luminescence sensitization. Photophysical properties of all complexes were analyzed by optical spectroscopy and an energy transfer scheme was discussed. A combination of two types of ligands into the coordination sphere (phosphate and phenanthroline) allows designing the Eu surrounding with very high intrinsic quantum yield Q_{Eu}^{Eu} (0.92) and highly luminescent Ln complexes for both visible and near-infrared (NIR) regions.

Keywords: lanthanides; luminescence; crystal structure; organophosphate ligands; N-ligands

1. Introduction

The development of highly luminescent compounds that are potentially applicable in modern optical materials is still a great challenge due to the rapidly evolving requirements of practical life [1,2]. In coordination chemistry of lanthanide elements, the key role among organic ligands has always belonged to carboxylates [3,4]. Meanwhile, related organophosphorus ligands (phosphonates, phosphinates, and phosphoric esters), which can coordinate a Ln^{3+} cation as mono- and polydentate ligands, also have great potential for the formation of complexes with 4f elements. Lanthanide complexes with organophosphate ligands should be more resistant to hydrolysis due to the higher acidity of phosphoric acids, compared with carboxylic acids. However, these complexes, and especially their crystal structures, remain virtually unexplored. There are only a few examples of the use of aryl phosphate as a ligand in the coordination chemistry of lanthanides. Various lanthanide complexes

with disubstituted organophosphate ligands are currently being studied, for example, as precatalysts for various catalytic processes, including polymerization of conjugated dienes [5–9].

Another attractive side of aryl phosphate complexes is the presence of a conjugated system within the ligand. Such ligands are capable of efficiently absorbing electromagnetic radiation and therefore can be considered as potential “antenna ligands” for sensibilization of the lanthanide luminescence [10,11]. There are no examples of an application of organophosphate ligands for 4f-ions luminescence sensitization. Moreover, the aryl phosphate Ln complexes are an example of a system with electronic separation between the energy-donating aromatic orbital and the energy-accepting Ln^{3+} orbital via a spacer with low vibrational frequency [12]. This separation is expected to suppress the vibrational relaxation of the Eu^{3+} ion and to induce an effective energy transfer determined by the weak electronic interaction between the energy donor (aromatic ligand) and the acceptor (Eu^{3+}). Quenching of the Ln^{3+} luminescence by high-energy vibrations (typically X-H oscillators, X = C, N, O) plays an important role, especially in the case of the Eu ion, owing to the energy gap law [13]. On the other hand, aryl phosphate are bulky ligands and the introduction of several ligands into the Ln^{3+} coordination sphere can lead to substantial steric hindrances. To overcome this, we used the Cl^- anion as the second type of the counterion. Moreover, chloride by being a single atom turns out to be a very efficient ligand dissimilarity enhancer and coordination symmetry breaker, which can boost luminescence in a significant manner [14].

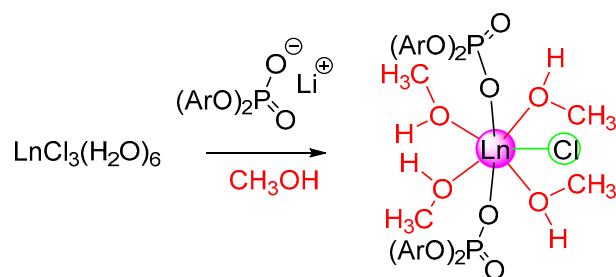
Therefore, the sterically crowded bis((2,6-diisopropyl)phenyl)phosphate ligand was taken as a first example of an Ln system containing disubstituted organophosphate for design of new Ln complexes for luminescence applications.

The present article is focused on the synthesis of mononuclear heteroleptic lanthanide organophosphate complexes of Nd, Eu, Gd, Tb, and their terpyridine and phenanthroline adducts, as well as on investigations of their molecular structure and luminescence properties. Photophysical properties of these compounds are discussed based on experimental data of singlet and triplet levels, lifetimes of excited states, integrated intensities of electronic transitions parameters, radiative (k_r) and non-radiative rate constant (k_{nr}), and overall and intrinsic quantum yields (Q_{Ln}^{Lig} , Q_{Eu}^{Eu}).

2. Results and Discussion

2.1. Bis-((2,6-Diisopropyl)Phenyl)Phosphate Lanthanide Complexes, Synthesis, and Photophysical Properties

Reactions of $\text{LnCl}_3(\text{H}_2\text{O})_6$ with 2 equivalents of lithium (2,6-diisopropyl) phosphate in dry methanol led to the corresponding bis(2,6-diisopropylphenyl)phosphate complexes (Scheme 1). Recrystallization of europium (2), gadolinium (3), and terbium (4) complexes from methanol allowed obtaining crystals suitable for single-crystal X-ray diffraction analysis.



Scheme 1. Synthesis of bisorganophosphates 1–4, Ar = (2,6-diisopropyl)phenyl, Ln = Nd (1), Eu (2), Gd (3), and Tb (4).

The structures of 2–4 (Figure 1) are isomorphous with the previously described ones for complexes $\{[\text{Ln}(\text{O}_2\text{P}(\text{OAr})_2)_2\text{Cl}(\text{CH}_3\text{OH})_4]\cdot\text{MeOH}\}$ (Ln = Nd (1), Y, Lu; Ar = O-2,6-iPr₂C₆H₃) [9]. Four methanol

molecules, the chloride anion, and two organophosphate ligands exhibit the κ^1 -O-terminal coordination mode (Figure 1) coordinate Ln³⁺ cation.

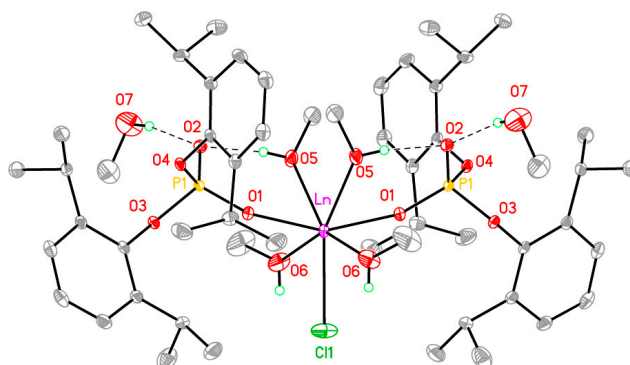


Figure 1. The crystal structures of 2–4 (using 2 as an example). Here and after, ellipsoids are drawn at 50% probability level.

The closest polyhedron for the metal environment is a distorted pentagonal bipyramid with two O1 organophosphate atoms being in axial positions. The Ln-OP bond lengths are shorter by ~ 0.14 Å than the Ln-OMeOH ones (Table 1). Two intermolecular O₅-H₂₈...O₂ bonds form 6-membered rings connecting the organophosphate ligand and a coordinated methanol molecule. Intermolecular OH...O hydrogen bonds (O₆-H₂₉...O₇, O₇-H₃₀...O₂) form a 2D OH...O hydrogen bond framework (see SI for details), which results in low solubility of these complexes in commonly used organic solvents.

Table 1. Selected bond lengths for 2–4 (Å).

	2 (Eu)	3 (Gd)	4 (Tb)
Ln-O1	2.2947 (10)	2.286 (2)	2.2669 (10)
Ln-O5	2.4366 (11)	2.422 (3)	2.4068 (12)
Ln-O6	2.4360 (12)	2.425 (3)	2.4086 (13)
Ln-Cl	2.6458 (6)	2.6443 (15)	2.6290 (6)

2.2. Adducts of Bis- and Trisdiisopropylphenylphosphate Complexes with Terpyridine

The interaction of bis(diisopropylphenyl phosphates) 2–4 with an equivalent amount of terpyridine led to the formation of 1:1 adducts $[(2,6\text{-}i\text{-Pr}_2\text{C}_6\text{H}_3\text{O})_2\text{PO}_2]_2\text{LnCl}(\text{ter-pyridine})(\text{H}_2\text{O})_2(\text{CH}_3\text{OH})$ Ln = Eu (5), Gd (6), and Tb (7) (Scheme 2). The molecular structure of 5 was resolved by X-ray studies (Figures 2 and 3). We were unable to obtain X-ray quality single crystals of 6 and 7; nevertheless, the fact that the IR spectra of complexes 5–7 are identical (Figures S10–S12) suggests that 6 and 7 are isostructural with 5.

In the case of Nd complex 1, the reaction with terpyridine was accompanied by ligands metathesis and led to the formation of a tris(diarylphosphate) complex $[(2,6\text{-}i\text{-Pr}_2\text{C}_6\text{H}_3\text{O})_2\text{PO}_2]_3\text{Nd}(\text{ter-pyridine})(\text{H}_2\text{O})(\text{CH}_3\text{OH})$ (8) (Scheme 3), the structure of which was also established by X-ray diffraction analysis (Figure 4). It should be noted that all terpyridine complexes contain two (complexes 5–7) or one (complex 8) water molecules coordinated with the lanthanide cation. The composition of the complexes according to X-ray diffraction data (Table S1) is in a good agreement with microanalytical data for samples taken from the bulk of the substance. The most likely source of water may be residual water in toluene. Attempts to isolate terpyridine complexes that do not contain coordinated water molecules have been unsuccessful.

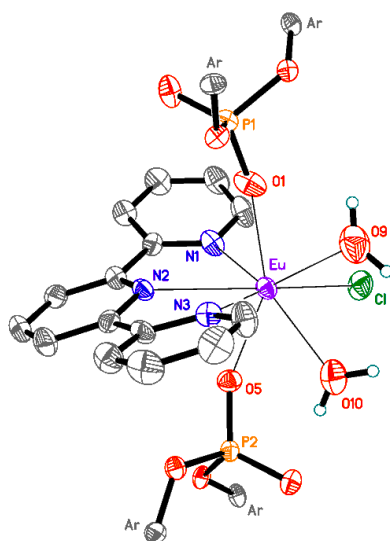
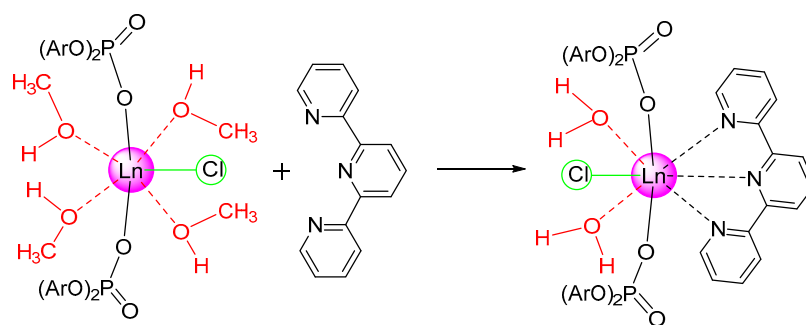
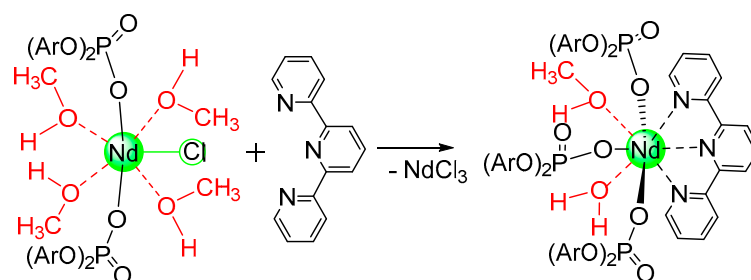


Figure 2. The crystal structures of **5**. A non-coordinating methanol molecule is omitted. Only ipso carbon atoms of aryl groups, labeled as Ar, are shown for clarity.



Scheme 2. Synthesis of complexes **5–7**, Ln = Eu (**5**), Gd (**6**), Tb (**7**).

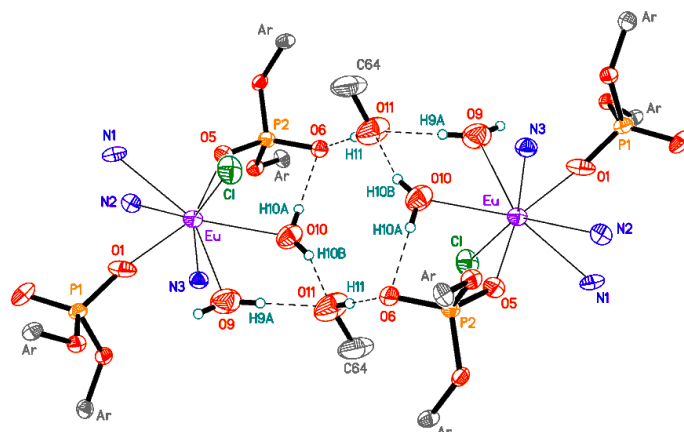


Scheme 3. Synthesis of complex **8**.

Two methanol molecules present in **2** (Figure 1) are replaced in **5** (Figure 2) with a terpyridine ligand, increasing the Eu^{3+} coordination number from 7 to 8. The $\text{Eu}-\text{O}_\text{P}$ bond lengths in **5** remain nearly the same ($\text{Eu}-\text{O}5$) or are slightly decreased by 0.04 \AA ($\text{Eu}-\text{O}1$) as compared with $\text{Eu}-\text{O}_\text{P}$ in **2** (Tables 1 and 2), whereas the $\text{Eu}-\text{Cl}$ bond is elongated by 0.04 \AA , and the $\text{Eu}-\text{O}_\text{water}$ lengths are $\sim 0.07 \text{ \AA}$ larger than the $\text{Eu}-\text{O}_\text{MeOH}$ ones in **2**. The terpyridine ligand display different dihedral angle values for the planes formed by two neighboring six-membered rings: $22.0(4)^\circ$ for the ring containing N1 and $8.7(5)^\circ$ for the group with N3 with respect to the middle ring. Two neighboring molecules $[(\text{O}_2\text{P}(\text{OAr})_2)_2\text{EuCl}(\text{H}_2\text{O})_2(\text{terpy})]$ form a dimeric associate $\{[(\text{O}_2\text{P}(\text{OAr})_2)_2\text{EuCl}(\text{H}_2\text{O})_2(\text{terpy})]_2(\text{MeOH})_2\}$ located on an inversion center via intermolecular hydrogen bonding involving non-coordinating methanol molecules (Figure 3 and Supplementary Information).

Table 2. Selected bond lengths for **5** (Å).

Bond Length		Bond Length	
Eu-O1	2.252 (5)	Eu-N1	2.558 (6)
Eu-O5	2.291 (5)	Eu-N3	2.565 (6)
Eu-O9	2.496 (6)	Eu-N2	2.601 (6)
Eu-O10	2.515 (6)	Eu-Cl	2.6850 (19)

**Figure 3.** Formation of dimeric moiety $\{[(O_2P(OAr)_2)_2EuCl(H_2O)_2(terpy)]_2(MeOH)_2\}$ in **5** via hydrogen bonding. Carbon atoms of the terpyridine ligand are not shown.

In some respect, product **8** $[(O_2P(OAr)_2)_3Nd(MeOH)(H_2O)(terpy)]$ (Figure 4) might be formally considered as a substitution product of complex $[(O_2P(OAr)_2)_3Nd(MeOH)_5]$ [15], in which four coordinated methanol molecules are replaced by terpyridine and water molecules, retaining the Nd^{3+} coordination number of 8. Indeed, the interaction of $[(O_2P(OAr)_2)_3Nd(MeOH)_5]$ with terpyridine resulted in the formation of **8** with the higher yield in comparison with the reaction of **1** with terpyridine. The $Nd-O_P$ distances in **8** (Table 3) are on average shorter by ~ 0.02 Å than those in $[(O_2P(OAr)_2)_3Nd(MeOH)_5]$. The $Nd-O_{MeOH}$ and $Nd-O_{water}$ distances in **8** lie in the range found for $Nd-O_{MeOH}$ bonds in $[(O_2P(OAr)_2)_3Nd(MeOH)_5]$ (2.469(2)–2.537(2) Å, average 2.497 Å) [6]. The values of interplanar angles between neighboring rings of the terpyridine ligand are $18.53(11)^\circ$ and $22.22(7)^\circ$. Complex **8** exhibits three intermolecular $OH\cdots O$ hydrogen bonds (Figure 4 and Supplementary Information).

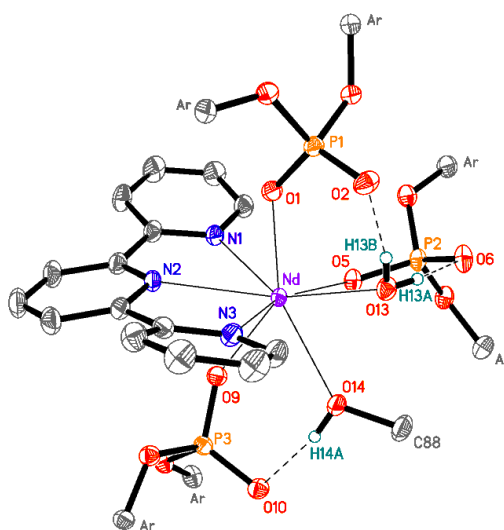
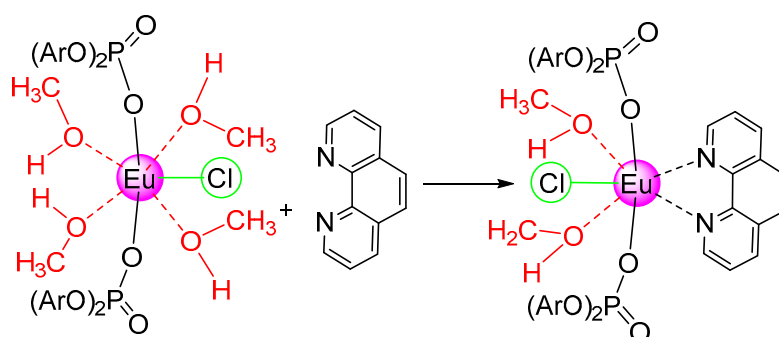
**Figure 4.** The crystal structure of **8**.

Table 3. Selected bond lengths for **8** (Å).

Bond Length		Bond Length	
Nd-O1	2.3993 (16)	Nd-O14	2.5208 (16)
Nd-O5	2.3512 (16)	Nd-N1	2.6339 (19)
Nd-O9	2.3638 (16)	Nd-N2	2.6477 (19)
Nd-O13	2.5124 (17)	Nd-N3	2.599 (2)

Each phosphate anion in compounds **2–5** and **8** demonstrates that two P-O_{Ar} bonds are longer by 0.09–0.11 Å than the other two P-O distances (see SI), and the smallest O-P-O angle value corresponds to the O_{Ar}-P-O_{Ar} angle between two bulky aryl ligands.

To compare the effectiveness of various N-heterocyclic “antenna ligands”, an Eu bis (di-isopropyl phosphate)-chloride complex with phenanthroline was synthesized. The reaction of **2** with phenanthroline led to the formation of **9** (Scheme 4).

**Scheme 4.** Synthesis of complex **9**.

We were unable to obtain a single-crystal of **9** appropriate for X-ray analysis. Nevertheless, the spectral characteristics of the complexes prove the presence of an N-heterocyclic ligand in the coordination sphere of the Eu³⁺ cation.

2.3. Photophysical Properties

The europium ion is well known as a perfect probe for chemical surroundings, owing to its electronic configuration [16–18]. The luminescence spectra of the Eu complexes studied demonstrate the characteristic transitions of the Eu³⁺ ion from the excited state ⁵D₀ to the ground state ⁷F_J (J = 0–4) as well as from the ⁵D₁ state in the complex **9** (Figure 5). The ⁵D₀ → ⁷F_J (J = 0–4) transitions display the maximum possible number of Stark components in the complexes **5** and **9**, pointing to low site symmetry for the Eu³⁺ ion, i.e., equal to or lower than C_{2v}. The splitting patterns of these transitions are similar in complexes **5** and **9**, while they are completely different in complex **2**. These data are confirmed by peculiarities of the coordination spheres in these complexes. Indeed, in complex **2** a coordination sphere is formed by six oxygen atoms and one chlorine atom, whereas four oxygen atoms, two nitrogen atoms, and one chlorine atom form the coordination sphere in complex **9**. Furthermore, this finding also correlates with XRD data according to which the Eu ion has different site symmetry, i.e., special position (C2) in **2** and general position in **5**. The ⁵D₀ → ⁷F₀ transition is strictly forbidden according to the standard Judd–Ofelt theory, and the most obvious explanation why this transition is observed is to assume that this transition is due to J-mixing or to mixing of low-lying charge-transfer states into the wavefunctions of the 4f⁶ configuration [16]. In the luminescence spectra, the ⁵D₀ → ⁷F₀ transition (region: 570–585 nm) is presented as a single symmetrical line, indicating the presence of only one type of the luminescence center in all complexes. The intensity of the magnetic dipole ⁵D₀ → ⁷F₁ transition is largely independent of the europium ion environment. The ratios of the integrated intensities of the europium electronic transitions to the integrated intensity of magnetic dipole transition ⁵D₀ → ⁷F₁

estimated from the luminescence spectra of the Eu complexes are given in Table 4. The lowest ratio obtained for the ${}^5D_0 \rightarrow {}^7F_0$ transition (0.01) in complex 9 could be a result of the most symmetric charge arrangement around the Eu^{3+} ion. The highest ratio (0.05) was found in complex 2. Assuming the data about site symmetry of the Eu^{3+} ion in 2 and 9, the presence of the low-lying charge-transfer states can be proposed. The lowest ratio obtained for the ${}^5D_0 \rightarrow {}^7F_2$ transition (3.26) in complex 5 reveals the symmetry site of the Eu^{3+} ion nearby to the inversion center. A similar value for this ratio was determined for binuclear europium pivalate and acetate with phenanthroline [19,20].

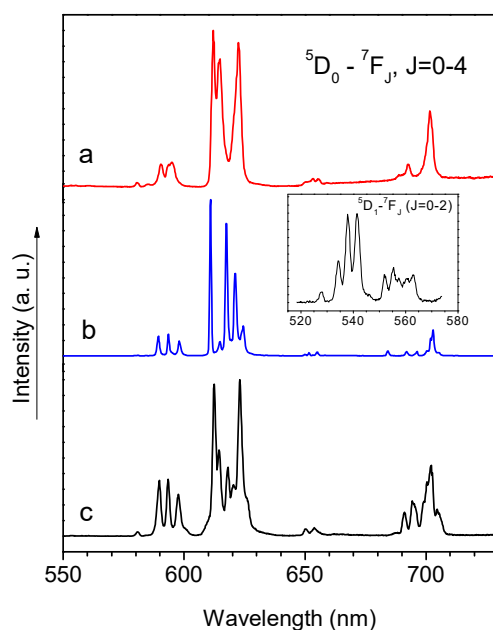


Figure 5. Luminescence spectra of Eu complexes 2 (a), 9 (b), and 5 (c) at 77 K, $\lambda_{\text{exc}} = 390$ for panel (a) and 340 nm for panels (b,c).

Table 4. The ratio of the integrated intensities of the ${}^5D_0\text{-}{}^7F_J$ ($J = 0, 2, 4$) transitions of the Eu^{3+} ion to the integrated intensity of the ${}^5D_0 \rightarrow {}^7F_1$ transition.

Complex	${}^5D_0\text{-}{}^7F_0$	${}^5D_0\text{-}{}^7F_2$	${}^5D_0\text{-}{}^7F_4$	Total
2	0.05	6.55	1.87	9.89
5	0.03	3.26	1.03	5.51
9	0.01	6.64	0.97	8.87

The luminescence decay curves were measured for all Eu and Tb complexes and they were fitted with a single exponential function. The lifetime values (τ) of the 5D_0 emitting level are presented in Table 5. The longest τ value at 300 K between Eu complexes was found for complex 9 (1.77 ± 0.03 ms), while the shortest one was observed for the complex 2 (0.28 ± 0.01 ms).

Table 5. Energy of S1 and T1 states, observed lifetimes, values of energy gaps E1 and E2, as well as intrinsic ($Q_{\text{Eu}}^{\text{Eu}}$) and overall ($Q_{\text{Eu}}^{\text{Lig}}$) quantum yields ^a.

	τ_{obs} , ms	S1, nm/cm ⁻¹	T1, nm/cm ⁻¹	E1, cm ⁻¹	E2, cm ⁻¹	$Q_{\text{Eu}}^{\text{Eu}}$ ^b	$Q_{\text{Eu}}^{\text{Lig}}$
2	0.28 ± 0.01	275/36,350	395/25,300	11050	8100	0.13	0.01
5	0.61 ± 0.02	355/28,170	440/22,730	5440	5530	0.17	0.11
9	1.77 ± 0.02	350/28,570	450/22,200	6370	5000	0.92	0.39

^a All photophysical data were measured at ambient temperature; ^b intrinsic quantum yield was calculated by Equation (3), values of quantum yield are given in fraction.

To understand the latter, the radiative rate constant k_r and non-radiative rate constant k_{nr} were calculated as $4.57 \times 10^2 \text{ s}^{-1}$ and $31.79 \times 10^2 \text{ s}^{-1}$, respectively, and the large k_{nr} is probably caused by photoinduced electron transfer process (see Equation (4)). The long lifetime found in **9** can be a consequence of the absence of such effective luminescence quenchers as OH oscillators from coordinated water molecules, while the presence of coordinated methanol molecules affects it to a lesser degree, owing to the ability to form strong hydrogen bonds with PO groups and longer distance Ln-O. The shorter lifetime obtained for complex **5** ($0.61 \pm 0.02 \text{ ms}$) corresponds to the presence of four O-H oscillators coordinated as well as the increasing lifetime at 77 K ($1.08 \pm 0.02 \text{ ms}$). The longer lifetime of the Tb^{3+} ion in complex **7** in comparison with one for the Eu^{3+} ion in corresponding compound **5** (1.31 ± 0.02 vs. $0.61 \pm 0.02 \text{ ms}$) is expected considering the energy gap law [13].

Despite the short lifetime of the Eu^{3+} ion in complex **2**, the luminescence spectrum for isostructural Tb complex was obtained. The Tb complex **4** shows the emission spectrum with typical narrow band ascribed to the terbium transitions $^5\text{D}_4 \rightarrow ^7\text{F}_5$ (489 nm), $^5\text{D}_4 \rightarrow ^7\text{F}_5$ (543 nm), $^5\text{D}_4 \rightarrow ^7\text{F}_4$ (585 nm), $^5\text{D}_4 \rightarrow ^7\text{F}_3$ (619 nm), $^5\text{D}_4 \rightarrow ^7\text{F}_2$ (645 nm), $^5\text{D}_4 \rightarrow ^7\text{F}_1$ (665 nm), and $^5\text{D}_4 \rightarrow ^7\text{F}_0$ (694 nm) (Figure S2). The overall quantum yield $Q_{\text{Tb}}^{\text{Lig}}$ for Tb complex **4** is equal to 10%. The Tb complex **7**, which is isostructural to Eu complex **5**, shows the emission spectrum with a typical narrow band ascribed to the terbium transitions $^5\text{D}_4 \rightarrow ^7\text{F}_j$ ($j = 5-0$) (Figure S3) as well. The transition $^5\text{D}_4 \rightarrow ^7\text{F}_5$ is the most intense transition in this spectrum and consists 44% of total integrated intensity. The Nd complex **8** also exhibits typical luminescence with peaks centered at 900, 1080, and 1320 nm, which correspond to the $^4\text{F}_{3/2} \rightarrow ^4\text{I}_{9/2}$, $^4\text{F}_{3/2} \rightarrow ^4\text{I}_{11/2}$, and $^4\text{F}_{3/2} \rightarrow ^4\text{I}_{13/2}$ transitions of the Nd^{3+} ion upon excitation through ligand absorption bands (Figure S4). The $^4\text{F}_{3/2} \rightarrow ^4\text{I}_{11/2}$ transition is dominant and consists of ~45% of the total intensity. Therefore, the usage of diarylphosphate ligand in combination with N-heterocyclic ligands allows to obtain the strong luminescence for visible and near-infrared (NIR) regions.

As the complexes studied are potentially interesting in different optical applications such parameters as the luminance and the ways of its improvement are important. According to the concept of sensitized luminescence, energy absorbed by ligands is transferred via singlet (S_1) and triplet (T) states to the excited levels of the lanthanide ion. In the case of the complexes containing the Tb^{3+} ion, the probability of the occurrence of the back energy transfer (BET) process is also high. Moreover, the presence of donor and acceptor fragments within a ligand can cause the charge redistribution upon the excitation and leads to intraligand charge transfer (ILCT) state. Such states were observed in the excitation spectra of lanthanide pyridine carboxylates and dicarboxylates [21–23]. In these complexes, the dependence of frequency of ILCT band as the function of isomer as well as on the coordination manner of carboxylate groups was discovered. The supramolecular network of H-bonds and π -stacking interactions can also induce sizeable charge redistribution within ligands and solvent molecules and affect the lanthanide surroundings. As a result of such charge redistribution, ILCT state appears and participates in the sensitization of Ln^{3+} ion luminescence. It should be noted also that in the case of Eu complexes, owing to the low redox potential of this ion, the ligand to metal charge transfer (LMCT) state may have low energy and cause the luminescence quenching [17,18]. Therefore, the energies of S_1 and T states are very important for the optimization of intraligand energy transfer, but charge transfer states can also have a dramatic influence on the efficiency of this transfer.

The luminescence excitation spectra of complexes **2** and **4** containing only organophosphate ligands exhibit narrow lines of f-f transitions of the Eu^{3+} and Tb^{3+} ions respectively (Figure 6c,d). The comparison of these excitation spectra reveals the presence of two intense bands in the region 250–380 nm in the excitation spectrum of Tb complex **4**. The first one is centered around 275 nm/ $36,350 \text{ cm}^{-1}$ and can be assigned to transitions mainly attributed to the phenyl ring [24]. However, the presence of the f-d transition in this region cannot be excluded. The second broad band with a lower intensity is observed in the region 300–380 nm and its maximum was distinguished by multiple peaks fit procedure as ~325 nm/ $30,770 \text{ cm}^{-1}$. As a similar band is also present in the spectrum of Eu complex **2** at 77 K (Figure S1), it can be tentatively assigned to intra- or/and interligand charge

transfer due to the anion-assisted strong hydrogen bond between the coordinated methanol molecule and the P=O of the organophosphate ligand.

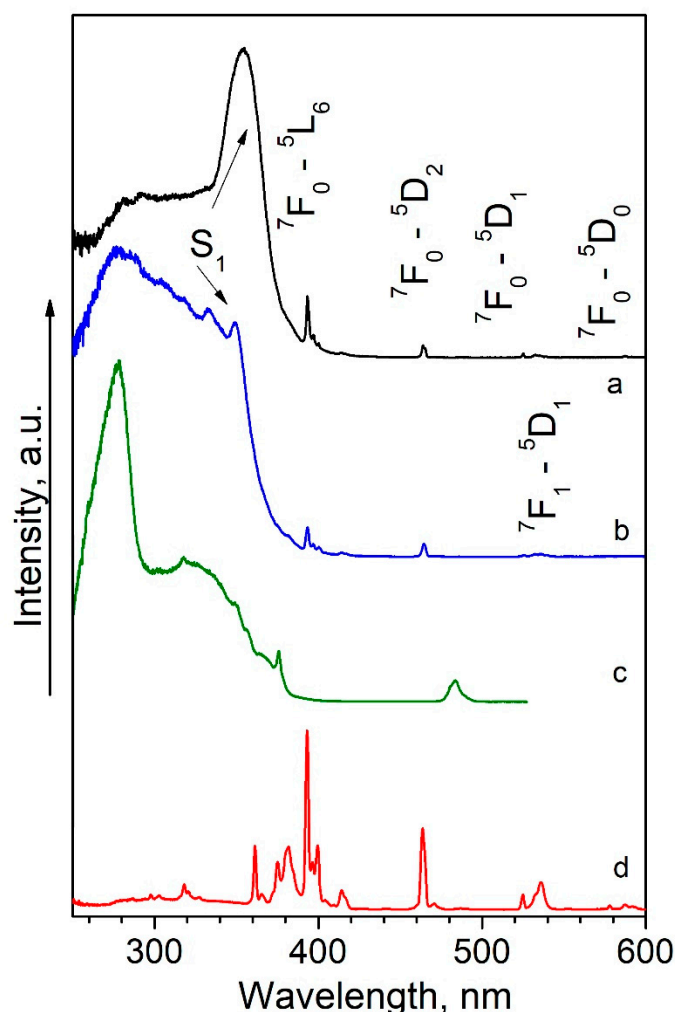


Figure 6. Luminescence excitation spectra of **5** (a), **9** (b), **4** (c), and **2**(d) at 300 K, $\lambda_{\text{reg}} = 615$ nm for Eu complexes (a,b,d) and 545 nm for Tb complex (c).

According to X-ray data, two intermolecular $\text{O}_5\text{-H}_{28}\cdots\text{O}_2$ bonds form 6-membered rings connecting the organophosphate ligand and coordinated methanol molecule. This hydrogen bond leads to the additional charge redistribution from anion to the neutral solvate molecule. Such charge redistribution determined by intermolecular interactions promotes the appearance of ILCT state. Similar charge redistribution caused by intermolecular $\text{H}\cdots\text{Cl}$ bonds, hydrogen bonds, and/or stacking interaction and resulted in additional CT state was previously observed for Ln chlorides with N-heterocyclic compounds and triflates [25]. It should be mentioned that the ligand excitation bands are almost absent in the Eu complex **2**, while both intense ligand excitation bands and the narrow bands arising from f-f transitions are present in the spectrum of terbium complex **4**. The latter indicates that complex **4** demonstrates the luminescence via direct and indirect excitation while the complex **2** only via direct excitation.

Previously, we have shown that the energy of $\text{Cl}^- \rightarrow \text{Eu}^{3+}$ CT state is ~ 340 nm in $[\text{EuCl}_2\text{bipy}_2(\text{H}_2\text{O})_2]\text{Cl}\cdot\text{H}_2\text{O}$, where the bond length of the Eu-Cl is equal to 2.71 \AA [25]. Taking into account the correlation between energy of the LMCT state and Eu-ligand bond length (the shorter the Eu-ligand bond length the shorter the wavelength of the charge-transfer band), and as the Eu-Cl

bond is remarkably shorter in complex **2** (2.65 Å), one can assume the energy of LMCT state should be higher. The presence of this LMCT state can be a reason for ineffective indirect excitation observed in complex **2** and discussed above large k_{nr} also confirms this interpretation. As the energy gaps E_1 and E_2 are very far also from optimal (Table 5), in order to improve the efficiency of energy transfer process in Ln complexes containing two organophosphate ligands we have introduced the second type of an “antenna”, namely, terpyridine and phenanthroline ligands (complexes **5** and **9**, respectively).

The luminescence excitation spectra of the Eu complexes **5** and **9** contain both narrow lines f-f transitions and intense broaden bands corresponding to the π - π^* and n - π^* transitions of heterocyclic aromatic ligands (terpyridine, phenanthroline) extending from 250 to 420 nm (Figure 6a,b). The maximum intensity of the Eu ion excitation through ligand bands is observed for the complex **9** with phen. The comparison of luminescence excitation spectra of the Eu, Gd, and Tb complexes with the terpyridine ligand (complexes **5**–**7**) reveals the presence of a broad band in the region 360–420 nm in the case of the Eu complex only (Figure 7). The maximum of this band was distinguished by multiple peaks fitting around ~ 380 nm/26,370 cm^{-1} nm (insert of Figure 7). The presence of this band only in the complex with the Eu ion allows its assignment to ligand \rightarrow metal charge transfer state. In complex of mononuclear europium thiocyanates with terpyridine the similar excited state was not found [26] and so LMCT state observed in **5** cannot be assigned to terpyridine ligand. Taking the energy of the LMCT state as 380 nm and the electronegativity of the Eu^{3+} ion uncorrected for spin correlation as $\chi_{\text{uncorr}}(\text{Eu}) = 1.99$ [27], it was possible to estimate the optical electronegativity of the ligand (χ_{opt}) participated in LMCT in **5** (see Equation (5)). The calculated value of (χ_{opt}) is 2.87 for **5** that is significantly different from the value estimated for the $\text{Cl}^- \rightarrow \text{Eu}^{3+}$ charge transfer state in $[\text{EuCl}_2\text{bipy}_2(\text{H}_2\text{O})_2]\text{Cl}\cdot\text{H}_2\text{O}$ (2.97) [25]. This difference is probably determined by cooperative effect of organophosphate ligand (having low optical electronegativity and high polarizability) and chloride anion.

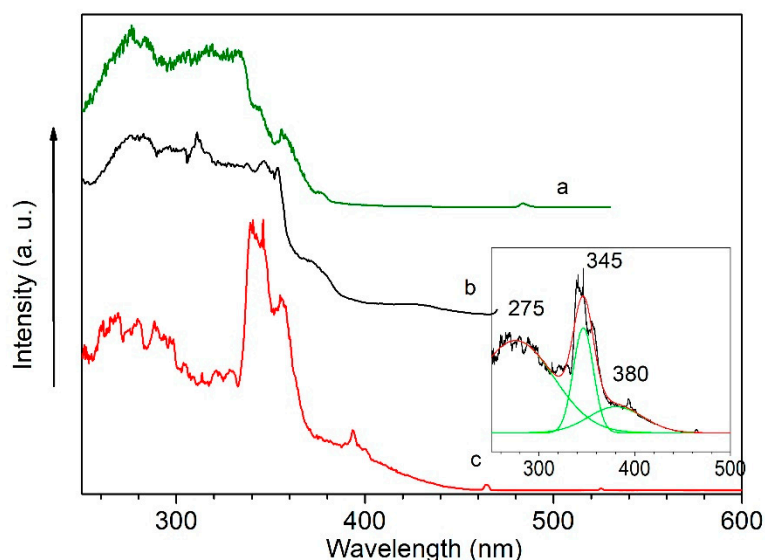


Figure 7. Luminescence excitation spectra of **7** (a), **6** (b) and **5** (c) at 77 K, $\lambda_{\text{reg}} = 545$ nm for (a), 490 nm for (b), and 615 nm for (c). Insert: multi-peaks fit of the luminescence excitation spectrum of **5** (c) performed by Origin 8.0.

The maximum of the lowest excited S_1 state is observed at 355 and 350 nm for terpyridine and phenanthroline complexes, respectively, and it was found that the values correlate well with ones published earlier [26,27]. Structural broad band with vibronic progression ~ 1380 cm^{-1} attributed to stretching vibration $\nu(\text{C}=\text{C}, \text{C}=\text{N})$ of phenanthroline ring observed in the region 310–350 nm of the luminescence excitation spectrum of complex **9** confirms the coordination of phenanthroline ligand. For the estimation of energy gaps E_1 and E_2 , the energy of T state was taken as 455 nm/22,400 cm^{-1} for

complex **9** [28] and as 439 nm/22,800 cm⁻¹ for complex **5** from the phosphorescence spectrum of Gd complex **6** (Figure S5). Therefore, energy gap E₁ equals to 5440 and 6370 cm⁻¹ for the Eu complexes **5** and **9**, respectively (Table 5), while E₂ is 5530 and 5000 cm⁻¹ for these complexes. Importantly, in Tb complex **7**, which is isostructural to complex **5**, the E₂ is 2330 cm⁻¹ only. In this case, the estimated E₂ value is near to limit and influence of BET process cannot be excluded. Previously BET influence on energy transfer process was demonstrated even at E₂ ~2489 cm⁻¹ [29].

The assignment of the bands in the luminescence excitation spectra along with experimentally determined energy of S₁ and T states allows us to decipher the energy transfer process in the complexes considered. In the complexes **2**, **5**, and **9** total quantum yield (Q_{Eu}^{Lig}) is equal to approximately 1, 11, and 39%, respectively (Table 5). The low value of Q_{Eu}^{Lig} obtained for complex **2** is reasonable taking into account that E₁ and E₂ gaps remarkably exceeds the optimum value (11,050 and 8100 cm⁻¹, respectively) as well as the presence of ILCT and LMCT states. In complex **5**, in spite of the optimal value for effective intersystem crossing process (energy gap E₁ is ~5440 cm⁻¹), the presence of two water molecules coordinated and the low-lying LMCT state (380 nm/26,320 cm⁻¹) lead to low value of intrinsic quantum yield (0.17), and therefore to low overall quantum yield Q_{Eu}^{Lig}. The significantly shorter lifetime of the excited ⁵D₀ state of the Eu³⁺ ion at 300 K in comparison with one for 77 K is in line with this interpretation. The high value of Q_{Tb}^{Lig} (0.45) in isostructural terbium complex **7** correlates well with the above explanation as the Tb ion is less sensitive to the presence of the O-H oscillators in the coordination sphere and LMCT state does not participate in the energy transfer process. The introduction of phosphate ligands into the coordination sphere along with phenanthroline ligand allows to design the Eu surrounding with a very high value of intrinsic quantum yield Q_{Eu}^{Eu}, which is 0.92 in the complex **9**. Such high value indicates that nonradiative processes are neglectable, the radiative rate constant k_r and non-radiative rate constant k_{nr} were calculated as 5.21 × 10² s⁻¹ and 0.44 × 10² s⁻¹, respectively. The high efficiency of the Eu ion excitation through ligand absorption bands observed in complex **9** along with high value of intrinsic quantum yield Q_{Eu}^{Eu} lead to relatively high overall quantum yield Q_{Eu}^{Lig} (0.39).

Interestingly that Eu complex with one phenanthroline ligand and chloride anions [EuCl₂Phen(H₂O)₄]Cl·H₂O studied [28] demonstrates lifetime of the ⁵D₀ level as 0.27 ± 0.02 ms vs. 1.77 ± 0.03 ms for complex **9** ([{(O₂P(OAr)₂)₂EuCl(CH₃OH)₂(phen)}]) and intrinsic quantum yield Q_{Eu}^{Eu} 0.08 vs. 0.92, respectively. This comparison allows to conclude that high intrinsic quantum yield in **9** is not solely the consequence of phenanthroline ligand introduction but the combination of phosphate ligand, chloride anion, and phenanthroline that is shown to be almost ideal from electronic and steric points of view for effective sensitization of the Eu³⁺ ion luminescence.

3. Materials and Methods

3.1. General Remarks

All described manipulations were conducted under argon using standard Schlenck and vacuum line techniques. Hydrated lanthanide chlorides LnCl₃(H₂O)₆ qualification “chemically pure” were used in the synthesis of complexes **1–4**. Argon was purified using columns with vermiculite impregnated with Mn^{II} oxide [30]. Tetrahydrofuran was predried over NaOH and distilled from potassium/benzophenone ketyl. Hexane was distilled from Na/K alloy/benzophenone ketyl. Toluene was distilled over sodium. [{(2,6-ⁱPr₂C₆H₃-O)₂POO}Li(MeOH)₃]·MeOH was prepared according to the previously described procedure [15] [{(2,6-ⁱPr₂C₆H₃-O)₂POO}₂NdCl(MeOH)₄]·2MeOH (**1**) was prepared according to literature [31]. Elemental analyses were performed with a Perkin-Elmer 2400 Series II elemental CHNS/O analyzer Perkin-Elmer, Billerica, MA, USA). The analysis of the complexes **4** and **9** for the content of carbon and hydrogen provides lower carbon values, likely resulting from the incomplete combustion and/or carbides formation, repeated experiments, using independently synthesized complexes results in the same values. The high-resolution mass spectra of **9** were recorded on a SolariX XR FT/ICR mass spectrometer (Bruker Daltonik GmbH, Bremen, Germany) equipped with a 15 T

superconducting magnet, a ParaCell analyzer cell, and an ESI Apollo II and MALDI SmartBeam-II ion source. External calibration of the mass spectrometer was performed using a low-concentration sodium trifluoroacetate solution (0.1 mg/mL in acetonitrile/water, 1:1). The data set size was 4M with 100 scans. All MALDI-FT-ICR-MS measurements were recorded in positive ion mode with MTP 384 ground steel target plate (3-indoleacrylic acid (IAA) matrix, with a scan range of m/z 150 to 3000). Twenty microliters of sample (10 $\mu\text{g/mL}$ in methanol) was mixed with 20 μL of 3-indoleacrylic acid (saturated solution in THF) using a pipette and placed onto a MTP 384 ground steel target plate (Bruker Daltonics, Bremen, Germany) and allow to dry at room temperature. All data visualization was processed using Data Analysis 5.1 software package from Bruker Daltonics (Billerica MS, USA). FTIR ATR spectra were measured on a Vertex 70v IR Fourier spectrometer (Bruker Optics, Ettlingen, Germany) using a Pike ATR accessory with a diamond crystal.

3.2. X-ray Crystallography

Single crystals of complexes **2–4** were isolated from the reaction mixtures. Crystals of **5** and **8** were obtained by slow diffusion of hexane into a toluene solution of the complexes. X-ray diffraction data for all studied complexes were collected on a SMART APEX II area-detector diffractometer (graphite monochromator, ω -scan technique) using $\text{MoK}\alpha$ -radiation (0.71073 Å). The intensity data were integrated by the SAINT program [32] and were corrected for absorption and decay using SADABS [33]. All structures were solved by direct methods using SHELXS [34] and were refined on F^2 using SHELXL [35]. All non-hydrogen atoms were refined with anisotropic displacement parameters. Positions of hydroxy and water H atoms in **2–4** and **8** were found from the electron density difference maps; these H atoms were refined with individual isotropic displacement parameters. All other hydrogen atoms were placed in ideal calculated positions and refined as riding atoms with relative isotropic displacement parameters taken as $U_{\text{iso}}(\text{H}) = 1.5U_{\text{eq}}(\text{C})$ for methyl groups and $U_{\text{iso}}(\text{H}) = 1.2U_{\text{eq}}(\text{C})$ otherwise. A rotating group model was applied for methyl groups. A highly disordered hexane molecule in **8** was removed by the SQUEEZE method [36]. The SHELXTL program suite was used for molecular graphics [33]. CCDC-1966199 (**2**), 1966200 (**3**), 1966201 (**4**), 1966202 (**5**), and 1966203 (**8**) contain the supplementary crystallographic data for this paper. These data can be obtained free of charge via <http://www.ccdc.cam.ac.uk/conts/retrieving.html> (or from the CCDC, 12 Union Road, Cambridge CB2 1EZ, UK; Fax: +44-1223-336033; E-mail: deposit@ccdc.cam.ac.uk). The crystallographic data and structure refinement details for **2–5** and **8** are given in Table S1 (See Supplementary Material ESI).

3.3. Synthesis and Characterization

3.3.1. Synthesis of $[(2,6\text{-}i\text{Pr}_2\text{C}_6\text{H}_3\text{-O})_2\text{POO}]_2\text{EuCl}(\text{CH}_3\text{OH})_4 \cdot 2\text{CH}_3\text{OH}$ (**2**)

$[(2,6\text{-}i\text{Pr}_2\text{C}_6\text{H}_3\text{-O})_2\text{POO}]\text{Li}(\text{CH}_3\text{OH})_3 \cdot \text{CH}_3\text{OH}$ (1.564 g (2.84 mmol)) was dissolved in 20 mL of dry CH_3OH and dropwise added to a 10 mL of a stirred solution of 0.538 g (1.42 mmol) of $\text{EuCl}_3 \cdot 6\text{H}_2\text{O}$ in CH_3OH , which led to the formation of a crystalline precipitate. The mixture was left in the freezer overnight. Several crystals were taken for X-ray studies. The precipitate was filtered off under argon, vacuum dried and recrystallized from methanol and then vacuum dried until the constant weight. The yield: 1.605 g (1.32 mmol, 93%) of **2**. Anal. calculated for $\text{C}_{54}\text{H}_{92}\text{P}_2\text{ClO}_{14}\text{Eu}$: C, 53.40%; H, 7.63%. Found: C, 52.15%; H, 8.25%. Complexes **3** and **4** were prepared in a similar way to the synthesis of **2**.

3.3.2. Synthesis of $[(2,6\text{-}i\text{Pr}_2\text{C}_6\text{H}_3\text{-O})_2\text{POO}]_2\text{GdCl}(\text{CH}_3\text{OH})_4 \cdot 2\text{CH}_3\text{OH}$ (**3**)

Following the same procedure, 1.660 g (3 mmol) of $[(2,6\text{-}i\text{Pr}_2\text{C}_6\text{H}_3\text{-O})_2\text{POO}]\text{Li}(\text{CH}_3\text{OH})_3 \cdot \text{CH}_3\text{OH}$, 0.588 g (1.5 mmol) of $\text{GdCl}_3 \cdot 6\text{H}_2\text{O}$ yielded 1.344 g (1.10 mmol, 74%). Anal. calculated for $\text{C}_{54}\text{H}_{92}\text{P}_2\text{ClO}_{14}\text{Gd}$: C, 53.16%; H, 7.60%. Found: C, 52.97%; H, 7.80%.

3.3.3. Synthesis of $[(2,6\text{-iPr}_2\text{C}_6\text{H}_3\text{-O})_2\text{POO}]_2\text{TbCl}(\text{CH}_3\text{OH})_4 \cdot 2\text{CH}_3\text{OH}$ (4)

Following the same procedure, 1.660 g (3 mmol) of $[(2,6\text{-iPr}_2\text{C}_6\text{H}_3\text{-O})_2\text{POO}]\text{Li}(\text{CH}_3\text{OH})_3 \cdot \text{MeOH}$ and 0.560 g (1.5 mmol) of $\text{TbCl}_3 \cdot 6\text{H}_2\text{O}$ yielded 1.638 g (1.34 mmol, 89%). Anal. calculated for $\text{C}_{54}\text{H}_{92}\text{P}_2\text{ClO}_{14}\text{Tb}$: C, 53.09%; H, 7.59%. Found: C, 51.84%; H, 8.33%.

3.3.4. Synthesis of $[(2,6\text{-iPr}_2\text{C}_6\text{H}_3\text{-O})_2\text{POO}]_2\text{EuCl}(\text{terpy})(\text{H}_2\text{O})_2(\text{CH}_3\text{OH})$ (5)

A toluene solution of 0.070 g (0.3 mmol) of terpyridine (terpy), was slowly added to a stirred solution of 0.304 g (0.25 mmol) of **2** in toluene. The reaction mixture was heated to a boil, and then it was slowly cooled to room temperature and left in a freezer overnight. The resulting precipitate was dried in vacuum to constant weight to yield 0.261 g (0.164 mmol, 66%) of **5**. Anal. calculated for $\text{C}_{64}\text{H}_{87}\text{N}_3\text{P}_2\text{ClO}_{11}\text{Eu}$: C, 58.07%; H, 6.62%; N, 3.17%. Found: C, 57.63%; H, 7.35%; N, 3.10%. IR (cm^{-1}) 3648 (w), 3064 (w), 2958 (s), 2865 (s), 1599 (m), 1575 (m), 1453 (s), 1437 (s), 1380 (w), 1329 (w), 1257 (m), 1208 (m), 1168 (m), 1072 (s), 1012 (w), 918 (m), 904 (m), 881 (w), 770 (m), 664 (w), 475 (w). MALDI-(+)MS $[\text{M}]^+$ = 1220.46074 Da, calculated for $\text{C}_{63}\text{H}_{79}\text{N}_3\text{P}_2\text{O}_8\text{Eu}$ = 1220.45492 Da, Δ = 4.8 ppm. $\text{C}_{63}\text{H}_{79}\text{N}_3\text{P}_2\text{O}_8\text{Eu}$ = (**5** - $2\text{H}_2\text{O}$ - CH_3OH - Cl^-) (Figure S15). X-ray quality crystals were obtained by slow diffusion of hexanes into the toluene solution of **5**. Compounds **6**–**7** were synthesized in a similar way to the synthesis of **5**.

3.3.5. Synthesis of $[(2,6\text{-iPr}_2\text{C}_6\text{H}_3\text{-O})_2\text{POO}]_2\text{GdCl}(\text{terpy})(\text{H}_2\text{O})_2(\text{CH}_3\text{OH})$ (6)

Terpyridine (0.070 g (0.3 mmol)), 0.558 g (0.25 mmol) of **3** yielded: 0.257 g (0.193 mmol, 77%) of **6**. Anal. calculated for $\text{C}_{64}\text{H}_{87}\text{N}_3\text{P}_2\text{ClO}_{11}\text{Gd}$: C, 57.84%; H, 6.60%; N, 3.16%. Found: C, 58.87%; H, 6.56%; N, 2.96%. IR (cm^{-1}) 3601 (w), 3065 (w), 2957 (s), 2866 (s), 1600 (m), 1575 (m), 1453 (s), 1437 (s), 1381 (w), 1330 (w), 1257 (m), 1210 (m), 1167 (m), 1075 (s), 1012 (w), 916 (m), 905 (m), 881 (w), 770 (m), 664 (w), 477 (w). MALDI-(+)MS $[\text{M}]^+$ = 1224.45889 Da, calculated for $\text{C}_{63}\text{H}_{79}\text{N}_3\text{P}_2\text{O}_8\text{Gd}$ = 1224.45839 Da, Δ = 0.4 ppm. $\text{C}_{63}\text{H}_{79}\text{N}_3\text{P}_2\text{O}_8\text{Gd}$ = (**6** - $2\text{H}_2\text{O}$ - CH_3OH - Cl^-). (Figure S16).

3.3.6. Synthesis of $[(2,6\text{-iPr}_2\text{C}_6\text{H}_3\text{-O})_2\text{POO}]_2\text{TbCl}(\text{terpy})(\text{H}_2\text{O})_2(\text{CH}_3\text{OH})$ (7)

Following the same procedure, 0.070 g (0.3 mmol) of terpyridine, 0.305 g (0.25 mmol) of **4** yielded 298 mg (0.187 mmol, 75%) of **7**. Anal. calculated for $\text{C}_{64}\text{H}_{87}\text{N}_3\text{P}_2\text{ClO}_{11}\text{Tb}$: C, 57.77%; H, 6.59%; N, 3.16%. Found: C, 57.65%; H, 7.84%; N, 3.10%. IR (cm^{-1}) 3641 (w), 3064 (w), 2956 (s), 2865 (s), 1599 (m), 1575 (m), 1453 (s), 1380 (w), 1329 (w), 1257 (m), 1209 (m), 1167 (m), 1076 (s), 1012 (w), 919 (m), 902 (m), 881 (w), 770 (m), 528 (w), 477 (w). MALDI-(+)MS $[\text{M}]^+$ = 1226.46134 Da, calculated for $\text{C}_{63}\text{H}_{79}\text{N}_3\text{P}_2\text{O}_8\text{Tb}$ = 1226.45905 Da, Δ = 1.8 ppm. $\text{C}_{63}\text{H}_{79}\text{N}_3\text{P}_2\text{O}_8\text{Tb}$ = (**7** - $2\text{H}_2\text{O}$ - CH_3OH - Cl^-) (Figure S17).

3.3.7. Synthesis of $[(2,6\text{-iPr}_2\text{C}_6\text{H}_3\text{-O})_2\text{POO}]_3\text{Nd}(\text{terpy})(\text{H}_2\text{O})(\text{CH}_3\text{OH})$ (8)

Route A. A toluene solution of 0.070 g (0.3 mmol) of 2,2':6',2''-terpyridine (terpy) was slowly added to a stirred solution of 0.25 mmol of **1** in toluene. The mixture was brought to a boil, slowly cooled to room temperature, and left in a freezer overnight. The mother liquor was removed and precipitate was dried in vacuum to constant weight to yield 0.243 g (0.144 mmol, 58%) of **8**. Anal. calculated for $\text{C}_{88}\text{H}_{119}\text{N}_3\text{P}_3\text{O}_{14}\text{Nd}$: C, 61.79%; H, 7.28%; N, 2.43%. Found: C, 61.73%; H, 7.13%; N, 2.65%. IR (cm^{-1}) 2963 (s), 2927 (w), 2866 (s), 1599 (m), 1575 (m), 1327 (w), 1254 (m), 1189 (m), 1168 (m), 1069 (s), 1045 (w), 1013 (w), 931 (m), 906 (m), 771 (m), 473 (w).

Route B. A toluene solution of 0.070 g (0.3 mmol) of 2,2':6',2''-terpyridine (terpy) was slowly added to a stirred solution of 0.397 g (0.255 mmol) of $[(\text{O}_2\text{P}(\text{OAr}))_3\text{Nd}(\text{MeOH})_5]$ in toluene. The mixture was brought to a boil, cooled to room temperature, and left in a freezer overnight. The precipitate formed was dried in vacuum to constant weight to yield 0.404 g (0.240 mmol, 94%) of **8**, which was identified by IR spectrum (Figure S13a), which was identical to the described above.

3.3.8. Synthesis of $[(2,6\text{-iPr}_2\text{C}_6\text{H}_3\text{-O})_2\text{POO}]_2\text{EuCl}(\text{phen})(\text{CH}_3\text{OH})_2$ (**9**)

Following the same procedure, 0.054 g (0.3 mmol) of o-phenantroline, 0.304 g (0.25 mmol) of **2** yielded: 198 mg (0.156 mmol, 62%) of **9**. Anal. calculated for $\text{C}_{62}\text{H}_{84}\text{N}_2\text{P}_2\text{ClO}_{10}\text{Eu}$: C, 58.79%; H, 6.68%; N, 2.21%. Found: C, 54.51%; H, 5.63%; N, 3.10%. IR (cm^{-1}) 3648 (w), 3063 (w), 2956 (s), 2865 (s), 2650 (s), 1598 (m), 1575 (m), 1453 (m), 1437 (m), 1380 (w), 1329 (w), 1257 (m), 1208 (m), 1167 (m), 1072 (s), 1012 (w), 918 (m), 903 (m), 881 (s), 769 (s), 664 (w), 528 (w), 473 (w). MALDI-(+)-MS $[\text{M}]^+ = 1167.462860$ Da, calculated for $\text{C}_{60}\text{H}_{76}\text{N}_2\text{P}_2\text{O}_8\text{Eu} = 1167.42929$ Da, $\Delta = 0.6$ ppm $\text{C}_{60}\text{H}_{76}\text{N}_2\text{P}_2\text{O}_8\text{Eu}^+ = (\mathbf{9} - 2\text{CH}_3\text{OH} - \text{Cl}^-)$ (Figure S18).

3.4. Optical Measurements

Steady-state luminescence and excitation measurements in the visible and NIR regions were performed with a Fluorolog FL 3-22 spectrometer (Horiba-Jobin-Yvon, Edison, NJ, USA) which has a 450 W xenon lamp as the excitation source and an R-928 photomultiplier. All optical measurements were performed for powdered samples. Only quartz capillaries were used for luminescence measurements. Time-resolved experiments, namely, luminescence lanthanide lifetimes (τ), were measured with initial delay = 0.05 ms, step size = 0.02 ms, and final window = 10 ms were measured at least three times, which were achieved by monitoring the decay at the maxima of the emission spectra. For phosphorescence spectrum initial delay = 0.1 ms. The single- or bi-exponential decays were analyzed with Origin[®] 8.1 (OriginLab Corporation, Northampton, MA, USA). The quantum yield measurements were carried out on solid samples with a Spectralone-covered G8 integration sphere (GMP SA, Renens, Switzerland) under ligand excitation, according to the absolute method of Wrighton [37–39]. Each sample was measured several times under slightly different experimental conditions. The estimated error for quantum yields was $\pm 10\%$. The values of quantum yield are given in fraction.

3.5. Calculation Based on Luminescence Data

The intrinsic luminescence quantum yields and the radiative (k_r) and nonradiative (k_{nr}) rate constants were estimated using equations as follows, [16,40,41]

$$\tau_r = \frac{1}{k_r} \quad (1)$$

$$\tau_{\text{obs}} = \frac{1}{k_r + k_{nr}} \quad (2)$$

$$Q_{\text{Eu}}^{\text{Eu}} = \frac{\tau_{\text{obs}}}{\tau_r} = \tau_{\text{obs}} \cdot A_{\text{MD},0} \cdot n^3 \cdot \left(\frac{I_{\text{tot}}}{I_{\text{MD},0}} \right) \quad (3)$$

where $A_{\text{MD},0}$ is the spontaneous luminescence probability for the ${}^5\text{D}_0 \rightarrow {}^7\text{F}_1$ transition in vacuum (14.65 s^{-1}), n is the refractive index of the medium, and $(I_{\text{tot}}/I_{\text{MD}})$ is the ratio of the total area of the Eu^{3+} luminescence spectrum to the area of the ${}^5\text{D}_0 \rightarrow {}^7\text{F}_1$ transition band. n was taken as 1.5 for all cases [41].

The overall deactivation rate constant, which is inversely proportional to the lifetime τk_{obs} is given by

$$k_{\text{obs}} = k^r + \sum_n k_n^{\text{nr}} = k^r + \sum_i k_i^{\text{vibr}}(\text{T}) + \sum_j k_j^{\text{pet}}(\text{T}) + \sum_k k_k^{\text{jnr}} \quad (4)$$

where k_r and k_{nr} are the radiative and non-radiative rate constants, respectively; the superscript “vibr” points to vibrational processes, while “pet” refers to photoinduced electron transfer processes; “jnr” are rate constants associated with remaining deactivation paths.

The energy of charge transfer state was estimated using by

$$E_{\text{CTS}} \cong 30\,000 \cdot [\chi_{\text{opt}}(\text{X}) - \chi_{\text{uncorr}}(\text{Eu})] \text{ cm}^{-1} \quad (5)$$

where $\chi_{\text{opt}}(X)$ and $\chi_{\text{uncorr}}(\text{Eu})$ are optical electronegativity of the ligand and uncorrected for spin correlation, respectively [16].

For energy gap calculations the energy of the ${}^5\text{D}_0$ and ${}^5\text{D}_4$ levels for Eu and Tb ions were taken as 17,300 and 20,500 cm^{-1} respectively.

4. Conclusions

The use of bis(diisopropylphenyl) phosphate-chloride ligand allowed to obtain a series of isomorphous heteroleptic complexes with a 7-coordinated Ln^{3+} cation. The interaction of complexes with terpyridine or phenanthroline leads to the formation of 1:1 adducts (Ln: N-containing ligand) with the simultaneous incorporation of water or methanol molecules into the coordination sphere of the Ln^{3+} ion. The luminescence intensity of organophosphosphate complexes themselves is low (quantum yields 0.01 and 0.1 for the Eu and Tb complexes); however, the introduction of N-containing ligand (terpyridine or phenanthroline) leads to a significant enhancement of luminescence ($Q_{\text{Ln}}^{\text{Lig}}$ 0.45 for Tb complex with terpyridine and 0.39 for Eu complex with phenanthroline). Moreover, the presence of two types of ligands in the coordination sphere (phosphate and phenanthroline) allows to design the Ln surrounding with very high intrinsic quantum yield $Q_{\text{Eu}}^{\text{Eu}}$ (0.92). It is worth emphasizing that a large volume of organophosphosphate ligand prevents the π -stacking interaction between N-containing ligands and relatively small coordination number (C.N. = 7) leads to shorter Ln-ligand bond lengths. These peculiarities of the organophosphosphate ligand promote high efficiency of the energy transfer process in the Ln complexes. In such a way, the performed study allows to conclude that diarylphosphate can be considered as a prospective ligand for the design of highly luminescent Ln complexes for both visible and NIR regions.

Supplementary Materials: The Supplementary Materials are available online. Figure S1. Luminescence excitation spectrum of Eu complex **5** at 77 K, $\lambda_{\text{reg}} = 615$ nm; Figure S2. Luminescence spectra of Tb complex (**4**) at 300 (a) and 77 K (b), $\lambda_{\text{exc}} = 320$ nm; Figure S3. Luminescence spectra of Tb complex (**7**) at 300 (a) and 77 K (b), $\lambda_{\text{exc}} = 320$ nm; Figure S4. Luminescence spectra of Nd complex (**8**) at 300 (a) and 77 K (b), $\lambda_{\text{exc}} = 320$ nm; Figure S5. Phosphorescence spectrum of Gd complex (**6**) at 77 K, $\lambda_{\text{exc}} = 320$ nm. *—transitions due to residual traces of Eu and Tb; Figure S6. Crystal structure of (**2**), (**3**) and (**4**), and hydrogen bonding; Figure S7. Crystal structure of (**5**); Figure S8. Hydrogen bonding in (**5**); Figure S9. Crystal structure of (**8**) and hydrogen bonding; Figure S10. IR spectrum of **5**; Figure S11. IR spectrum of **6**; Figure S12. IR spectrum of **7**; Figure S13. IR spectrum of **8**; Figure S13a. IR spectrum of **8** obtained from $[(\text{O}_2\text{P}(\text{OAr})_2)_3\text{Nd}(\text{MeOH})_5]$ (route B). (measured on a Ostec Ft-IR spectrometer); Figure S14. IR spectrum of **9**; Figure S15. Experimentally detected and theoretical MALDI-(+)MS spectrum of **5**; main experimental peak $[\text{M}]^+ = 1220.46074$ Da, calculated for $\text{C}_{63}\text{H}_{79}\text{N}_3\text{P}_2\text{O}_8\text{Eu} = 1220.45492$ Da, $\Delta = 4.8$ ppm. $\text{C}_{63}\text{H}_{79}\text{N}_3\text{P}_2\text{O}_8\text{Eu} = (5 - 2\text{H}_2\text{O} - \text{CH}_3\text{OH} - \text{Cl}^-)$; Figure S16. Experimentally detected and theoretical MALDI-(+)MS spectrum of (**6**); main experimental peak $[\text{M}]^+ = 1224.45889$ Da, calculated for $\text{C}_{63}\text{H}_{79}\text{N}_3\text{P}_2\text{O}_8\text{Gd} = 1224.45839$ Da, $\Delta = 0.4$ ppm. $\text{C}_{63}\text{H}_{79}\text{N}_3\text{P}_2\text{O}_8\text{Gd} = (6 - 2\text{H}_2\text{O} - \text{CH}_3\text{OH} - \text{Cl}^-)$; Figure S17. Experimentally detected and theoretical MALDI-(+)MS spectrum of (**7**); main experimental peak $[\text{M}]^+ = 1226.46134$ Da, calculated for $\text{C}_{63}\text{H}_{79}\text{N}_3\text{P}_2\text{O}_8\text{Tb} = 1226.45905$ Da, $\Delta = 1.8$ ppm. $\text{C}_{63}\text{H}_{79}\text{N}_3\text{P}_2\text{O}_8\text{Tb} = (7 - 2\text{H}_2\text{O} - \text{CH}_3\text{OH} - \text{Cl}^-)$; Figure S18. Experimentally detected and theoretical MALDI-(+)MS spectrum of (**9**); main experimental peak $[\text{M}]^+ = 1167.462860$ Da, calculated for $\text{C}_{60}\text{H}_{76}\text{N}_2\text{P}_2\text{O}_8\text{Eu} = 1167.42929$ Da, $\Delta = 0.6$ ppm. $\text{C}_{60}\text{H}_{76}\text{N}_2\text{P}_2\text{O}_8\text{Eu} = (9 - 2\text{CH}_3\text{OH} - \text{Cl}^-)$; Table S1. X-ray crystallographic data and refinement details for studied complexes; Table S2. Selected bond distances (Å) in (**2**), (**3**) and (**4**); Table S3. Hydrogen-bond geometry (Å, °) for (**2**), (**3**) and (**4**); Table S4. Selected bond distances (Å) in (**5**); Table S5. Hydrogen-bond geometry (Å, °) for (**5**); Table S6. Selected bond distances (Å) in (**8**); Table S7. Hydrogen-bond geometry (Å, °) for (**8**).

Author Contributions: Conceptualization, L.N.P., K.A.L. and D.M.R.; methodology, L.N.P. and D.M.R.; synthesis A.E.K., luminescence E.A.V. and I.V.T., crystallography K.A.L. and M.E.M.; resources, I.E.N.; data curation, L.N.P., D.M.R. and I.E.N.; writing—original draft preparation, M.E.M., L.N.P. and D.M.R.; writing—review and editing, L.N.P. and D.M.R.; funding acquisition, L.N.P. All authors have read and agreed to the published version of the manuscript.

Funding: This research was funded by Russian Science Foundation (grant No. 17-13-01357). Synthesis of precursors for organophosphate ligands was carried out within the State Program of TIPS RAS.

Acknowledgments: K.A.L. thanks RFBR grant No. 18-29-04029 for the support of the X-ray diffraction investigations. The authors are grateful to the Department of Structural Studies of the Zelinsky Institute of Organic Chemistry, Moscow, for performing HRMS experiments.

Conflicts of Interest: The authors declare no conflict of interest. The funders had no role in the design of the study; in the collection, analyses, or interpretation of data; in the writing of the manuscript; or in the decision to publish the results.

References

1. Bünzli, J.-C.G. Rising Stars in Science and Technology: Luminescent Lanthanide Materials. *Eur. J. Inorg. Chem.* **2017**, *2017*, 5058–5063. [[CrossRef](#)]
2. Bünzli, J.-C.G. Lanthanide Photonics: Shaping the Nanoworld. *Trends Chem.* **2019**, *1*, 751–762. [[CrossRef](#)]
3. Janicki, R.; Mondry, A.; Starynowicz, P. Carboxylates of rare earth elements. *Coord. Chem. Rev.* **2017**, *340*, 98–133. [[CrossRef](#)]
4. Ćcija, D.; Urgel, J.I.; Seitsonen, A.P.; Auwarter, W.; Barth, J.V. Lanthanide-Directed Assembly of Interfacial Coordination Architectures—From Complex Networks to Functional Nanosystems. *Acc. Chem. Res.* **2018**, *51*, 365–375. [[CrossRef](#)]
5. Minyaev, M.E.; Korchagina, S.A.; Tavgorkin, A.N.; Kostitsyna, N.N.; Churakov, A.V.; Nifant'ev, I.E. Crystal structures of mono- and binuclear neodymium diarylphosphate complexes and their catalytic activity in 1,3-diene polymerization. *J. Struct. Chem.* **2018**, *29*, 1475–1487. [[CrossRef](#)]
6. Nifant'ev, I.E.; Tavgorkin, A.N.; Korchagina, S.A.; Gavrilenko, I.F.; Glebova, N.N.; Kostitsyna, N.N.; Yakovlev, V.A.; Bondarenko, G.N.; Filatova, M.P. Neodymium tris-diarylphosphates: Systematic study of the structure–reactivity relationship in butadiene and isoprene polymerization. *Appl. Catal. A Gen.* **2014**, *478*, 219–227. [[CrossRef](#)]
7. Zhang, Z.; Cui, D.; Wang, B.; Liu, B.; Yang, Y. Polymerization of 1,3-Conjugated Dienes with Rare-Earth Metal Precursors. *Struct. Bond* **2010**, *137*, 49–108.
8. Nifant'ev, I.E.; Tavgorkin, A.N.; Shlyahin, A.V.; Korchagina, S.A.; Gavrilenko, I.F.; Glebova, N.N.; Churakov, A.V. Easily accessible, hydrocarbon-soluble, crystalline, anhydrous lanthanide (Nd, La, and Y) phosphates. *Dalton Trans.* **2013**, *42*, 1223–1230. [[CrossRef](#)]
9. Minyaev, M.E.; Tavgorkin, A.N.; Korchagina, S.A.; Bondarenko, G.N.; Churakov, A.V.; Nifant'ev, I.E. Isomorphous rare-earth tris-[bis-(2,6-diisopropylphenyl) phosphate] complexes and their catalytic properties in 1,3-diene polymerization and in the inhibited oxidation of polydimethylsiloxane. *Acta Cryst.* **2018**, *74*, 590–598.
10. Weissman, S.I. Intramolecular Energy Transfer The Fluorescence of Complexes of Europium. *J. Chem. Phys.* **1942**, *10*, 214–217. [[CrossRef](#)]
11. Bünzli, J.-C.G.; Piguet, C. Taking advantage of luminescent lanthanide ions. *Chem. Soc. Rev.* **2005**, *34*, 1048–1077. [[CrossRef](#)]
12. Kitagawa, Y.; Suzue, F.; Nakanishi, T.; Fushimi, K.; Hasegawa, Y. A highly luminescent Eu(III) complex based on an electronically isolated aromatic ring system with ultralong lifetime. *Dalton Trans.* **2018**, *47*, 7327–7332. [[CrossRef](#)]
13. Haas, Y.; Stein, G.; Tomkiewicz, M. Fluorescence and photochemistry of the charge-transfer band in aqueous europium(III) solutions. *J. Phys. Chem.* **1970**, *74*, 2558–2562. [[CrossRef](#)]
14. Silva, A.I.S.; Lima, N.B.D.; Simas, A.M.; Gonçalves, S.M.C. Europium Complexes: Luminescence Boost by a Single Efficient Antenna Ligand. *ACS Omega* **2017**, *2*, 6786–6794. [[CrossRef](#)] [[PubMed](#)]
15. Minyaev, M.E.; Nifant'ev, I.E.; Tavgorkin, A.N.; Korchagina, S.A.; Zeynalova, S.S. Crystal structure of [bis-(2,6-diisopropylphenyl) phosphato- κ O]tris-(methanol- κ O)lithium methanol monosolvate. *Acta Cryst. Sect. E Crystallogr. Commun.* **2015**, *71*, 443–446. [[CrossRef](#)] [[PubMed](#)]
16. Binnemans, K. Interpretation of europium(III) spectra. *Coord. Chem. Rev.* **2015**, *295*, 1–45. [[CrossRef](#)]
17. Bünzli, J.-C.G. On the design of highly luminescent lanthanide complexes. *Coord. Chem. Rev.* **2015**, *293–294*, 19–47. [[CrossRef](#)]
18. Carneiro Neto, A.; Teotonio, E.; de Sá, G.; Brito, H.; Legendziewicz, J.; Carlos, L.; Felinto, M.; Gawryszewska, P.; Moura, R.; Longo, R.; et al. Modeling intramolecular energy transfer in lanthanide chelates: A critical review and recent advances. In *Handbook on the Physics and Chemistry of Rare Earths*; Bünzli, J.-C., Pecharsky, V., Eds.; Elsevier: Amsterdam, The Netherlands, 2019; Volume 56, pp. 55–162.

19. Fomina, I.G.; Dobrokhotova, Z.V.; Kazak, V.O.; Aleksandrov, G.G.; Lysenko, K.A.; Puntus, L.N.; Gerasimova, V.I.; Bogomyakov, A.S.; Novotortsev, V.M.; Eremenko, I.L. Synthesis, Structure, Thermal Stability, and Magnetic and Luminescence Properties of Dinuclear Lanthanide(III) Pivalates with Chelating N-Donor Ligands. *Eur. J. Inorg. Chem.* **2012**, *22*, 3595–3610. [CrossRef]
20. Tsaryuk, V.I.; Legendziewicz, J.; Zolin, V.F.; Sokolnicki, J.; Szostak, R.; Puntus, L.N. Spectra and details of the structure of europium acetates with derivatives of 1,10-phenanthroline. *J. Alloys Compd.* **2001**, *323*, 661–666. [CrossRef]
21. Zolin, V.F.; Puntus, L.N.; Tsaryuk, V.I.; Kudryashova, V.A.; Legendziewicz, J.; Gawryszewska, P.; Szostak, R. Spectroscopy of europium and terbium pyridine-carboxylates. *J. Alloys Compd.* **2004**, *380*, 279–284. [CrossRef]
22. Puntus, L.N.; Zolin, V.F.; Babushkina, T.A.; Kutuza, I.B. Luminescence properties of isomeric and tautomeric lanthanide pyridinedicarboxylates. *J. Alloys Compd.* **2004**, *380*, 310–314. [CrossRef]
23. Puntus, L.N.; Zolin, V.F.; Kudryashova, V.A. Charge transfer bands in the Eu³⁺ luminescence excitation spectra of isomeric europium pyridine-dicarboxylates. *Phys. Solid State.* **2002**, *44*, 1440–1444. [CrossRef]
24. Puntus, L.N.; Chauvin, A.-S.; Varbanov, S.; Bunzli, J.-C.G. Lanthanide Complexes with a Calix [8] arene Bearing Phosphinoyl Pendant Arms. *Eur. J. Inorg. Chem.* **2007**, *2007*, 2315–2326. [CrossRef]
25. Puntus, L.N.; Lyssenko, K.A.; Pekareva, I.S.; Bunzli, J.-C.G. Intermolecular Interactions as Actors in Energy-Transfer Processes in Lanthanide Complexes with 2,2'-Bipyridine. *J. Phys. Chem. B* **2009**, *113*, 9265–9277. [CrossRef]
26. Petrosyants, S.P.; Ilyukhin, A.B.; Gavrikov, A.V.; Mikhлина, Y.A.; Puntus, L.N.; Varaksina, E.A.; Efimov, N.N.; Novotortsev, V.M. Luminescent and magnetic properties of mononuclear lanthanide thiocyanates with terpyridine as auxiliary ligand. *Inorg. Chim. Acta* **2019**, *486*, 499–505. [CrossRef]
27. Demirbilek, R.; Heber, J.; Nikitin, S.I. Charge transfer and 4fⁿ-4fⁿ⁻¹ 5d transitions of trivalent rare-earth ions in CsCdBr₃. Proceedings of XI Feofilov Symposium on Spectroscopy of Crystals Activated by Rare-Earth and Transition Metal Ions, Kazan, Russian Federation, 2001. *Proc. SPIE* **2002**, *4766*, 47–50.
28. Puntus, L.N.; Lyssenko, K.A.; Antipin, M.Y.; Bunzli, J.-C.G. Role of Inner- and Outer-Sphere Bonding in the Sensitization of Eu^{III}-Luminescence Deciphered by Combined Analysis of Experimental Electron Density Distribution Function and Photophysical Data. *Inorg. Chem.* **2008**, *47*, 11095–11107. [CrossRef]
29. Roitershtein, D.M.; Puntus, L.N.; Vinogradov, A.A.; Lyssenko, K.A.; Minyaev, M.E.; Dobrokhodov, M.D.; Taidakov, I.V.; Varaksina, E.A.; Churakov, A.V.; Nifant'ev, I.E. Polyphenylcyclopentadienyl Ligands as an Effective Light-Harvesting π -Bonded Antenna for Lanthanide +3 Ions. *Inorg. Chem.* **2018**, *57*, 10199–10213. [CrossRef]
30. Horvath, B.; Möseler, R.; Horvath, E.G.; Krauss, H.L. Über Oberflächenverbindungen von Übergangsmetallen. XI. Darstellung und Eigenschaften von Koordinativ ungesättigten Mangan(II)-Oberflächenverbindungen. *Z. Anorg. Allg. Chem.* **1975**, *418*, 1–16. [CrossRef]
31. Minyaev, M.E.; Nifant'ev, I.E.; Tavtorkin, A.N.; Korchagina, S.A.; Zeynalova, S.S.; Ananyev, I.V.; Churakov, A.V. Isomorphous rare-earth bis-[bis-(2,6-diisopropylphenyl)phosphate] complexes and their self-assembly into two-dimensional frameworks by intramolecular hydrogen bonds. *Acta Cryst. Sect. C Struct. Chem.* **2017**, *73*, 820–827. [CrossRef]
32. Bruker. Available online: <https://www.bruker.com/products/x-ray-diffraction-and-elemental-analysis/single-crystal-x-ray-diffraction/sc-xrd-software/apex3.html> (accessed on 26 August 2020).
33. Krause, L.; Herbst-Irmer, R.; Sheldrick, G.M.; Stalke, D. Comparison of silver and molybdenum microfocus X-ray sources for single-crystal structure determination. *J. Appl. Cryst.* **2015**, *48*, 3–10. [CrossRef] [PubMed]
34. Sheldrick, G.M. A short history of SHELX. *Acta Crystallogr. Sect. A Found. Crystallogr.* **2008**, *64*, 112–122. [CrossRef] [PubMed]
35. Sheldrick, G.M. Crystal structure refinement with SHELXL. *Acta Cryst. Sect. C Struct. Chem.* **2015**, *71*, 3–8. [CrossRef] [PubMed]
36. Spek, A.L. PLATON SQUEEZE: A tool for the calculation of the disordered solvent contribution to the calculated structure factors. *Acta Crystallogr. Sect. C Struct. Chem.* **2015**, *71*, 9–18. [CrossRef]
37. Wrighton, M.S.; Ginley, D.S.; Morse, D.L. Technique for the determination of absolute emission quantum yields of powdered samples. *J. Phys. Chem.* **1974**, *78*, 2229–2233. [CrossRef]
38. de Mello, J.C.; Wittmann, H.F.; Friend, R.H. An improved experimental determination of external photoluminescence quantum efficiency. *Adv. Mater.* **1997**, *9*, 230–232. [CrossRef]

39. Greenham, N.C.; Samuel, I.D.W.; Hayes, G.R.; Phillips, R.T.; Kessener, Y.A.R.R.; Moratti, S.C.; Holmes, A.B.; Friend, R.H. Measurement of absolute photoluminescence quantum efficiencies in conjugated polymers. *Chem. Phys. Lett.* **1995**, *241*, 89–96. [[CrossRef](#)]
40. Bunzli, J.-C.G. Lanthanide Luminescence for Biomedical Analyses and Imaging. *Chem. Rev.* **2010**, *110*, 2729–2755.
41. Werts, M.H.V.; Jukes, R.T.F.; Verhoeven, J.W. The emission spectrum and the radiative lifetime of Eu^{3+} in luminescent lanthanide complexes. *Phys. Chem. Chem. Phys.* **2002**, *4*, 1542–1548. [[CrossRef](#)]

Sample Availability: Samples of the compounds are not available from the authors.



© 2020 by the authors. Licensee MDPI, Basel, Switzerland. This article is an open access article distributed under the terms and conditions of the Creative Commons Attribution (CC BY) license (<http://creativecommons.org/licenses/by/4.0/>).